Results in Physics 56 (2024) 107138

Contents lists available at ScienceDirect

Results in Physics

journal homepage: www.elsevier.com/locate/rinp

Crystal structure, mechanical, electronic, optical and thermoelectric characteristics of Cs_2MCl_6 (M = Se, Sn, Te and Ti) cubic double perovskites

K. Bouferrache [a], M.A. Ghebouli [b], B. Ghebouli [c], Mohamed A. Habila [d], T. Chihi [b], M. Fatmi [b,*], A. Djemli [e], Mika Sillanpaa [f]

[a] Department of Physics, Faculty of Sciences, University of Mohamed Boudiaf, M'sila 28000, Algeria
[b] Research Unit on Emerging Materials (RUEM), University Ferhat Abbas of Setif 1, Setif, 19000, Algeria
[c] Laboratory for the Study of Surfaces and Interfaces of Solid Materials (LESIMS), University Ferhat Abbas of Setif 1, Setif 19000, Algeria
[d] Department of Chemistry, College of Science, King Saud University, P.O. Box 2455, Riyadh 11451, Saudi Arabia
[e] Faculty of Physics, University of Sciences & Technology Houari Boumediene (U.S.T.H.B), El Alia, BP 32, Bab Ezzouar, 16111 Algiers, Algeria
[f] Department of Biological and Chemical Engineering, Aarhus University, Norrebrogade 44, 8000 Aarhus C, Denmark

ARTICLE INFO

Keywords:
Crystal structure
Electronic characteristics
Cs_2MCl_6
Cubic double perovskites

ABSTRACT

The crystal structure, mechanical, electronic, optical and thermoelectric characteristics of Cs_2MCl_6 (M = Se, Sn, Te and Ti) cubic double perovskites are studied within GGA, GGA-mBJ and EV-GGA functionals. The M − Cl bond lengths are shorter and especially in Cs_2TiCl_6 double perovskite, which reflects the strong interaction between M and Cl atoms and this is correlated with its better chemical stability. The negativity of formation energy and Helmholtz free energy and no imaginary phonon modes throughout the Brillouin zone confirm the thermal, thermodynamic and dynamical stability of these double perovskites. Semiconductors Cs_2MCl_6 (M = Se, Sn, Te and Ti) double perovskites with flat conduction and valence bands, and an indirect band gap are p-type carriers. A high Seebeck coefficient, adequate ZT values and non-toxicity make these compounds attractive for thermoelectric applications at high temperature and spintronic technology. The empty first conduction band corresponds to their band gap, and the transition occurs from Cl-p to (Se-p, Sn-p, Te-p and Ti-d). The high static dielectric constant and the intense peak of the real part in the ultraviolet energy range favor less the recombination rate of charge carriers and their use in optoelectronic devices. The indirect band gap, high absorption in ultraviolet energy, high static refractive index make these cubic double perovskites as ideal materials for solar cell applications.

Introduction

We provide a study on the inorgaic hexachlorometallate structure, which has the general stoichiometric formula A_2MB_6, with the cubic antifluorite structure of space group $Fm\bar{3}m$. This series of double perovskites is attracting much attention from researchers because of their probable use as solar cells, photovoltaic absorbers, microwave semiconductor with a wide band gap and optoelectronic devices. We focus on double perovskites with the halide anion B = Cl and consider four compounds with varying M−site cations (Se, Sn, Te and Ti) and fixed the alcali metal A = Cs. This type of double perovskites called molecular salts show an ionic character because of their assembly of cations and anions. The structure of the Cs_2MCl_6 (M = Se, Sn, Te and Ti) is such that the "M" atoms are symmetrical fixed at (0, 0, 0) position 4a, the "Cl" atoms are at (x, 0, 0) position 24e (where, x is the anion positional parameter), and the "Cs" atoms are symmetrical fixed at (l/4, l/4, l/4) position 8c. Inorganic perovskites are materials where the conductivity is ensured by the transport of holes in solar cells based on mesoporous electrodes. The rapid evolution of inorganic perovskites materials is due to their use in solar cell and thermoelectric applications. The Cs_2MCl_6 lattice contains octahedral MCl_6^{2-} ions with 8 Cs cations, placed on the three axes. Each cation is in a tetrahedral site formed from four M atoms and has a symmetrical chlorine bond of 12. The M−Cl bond shows fourfold symmetry and is equivalent to the others. Regarding studies quoted by other researchers, M. Khuili et al. report a strong optical absorption in the ultraviolet region and adequate thermoelectric characteristics make Cs_2SnX_6 (X = Cl, Br, I) candidates for replacing expensive silicon cells in solar panels [1]. The electronic nature of Tl_2NbX_6 (X = Cl,

* Corresponding author.
E-mail address: fatmimessaoud@yahoo.fr (M. Fatmi).

https://doi.org/10.1016/j.rinp.2023.107138
Received 19 September 2023; Received in revised form 22 October 2023; Accepted 29 October 2023
Available online 23 November 2023

Table 1
The values of $R_{MT}xK_{max}$, R_{MT} of each constituent and k-point of Cs_2XCl_6 (X = Se, Sn, Te and Ti) double perovskites using GGA approaches.

type-I	R_{MT}xKmax	R_{MT} (Cs)	R_{MT} (X)	R_{MT} (Cl)	k-point
Cs2SeCl6	9	2.50	2.04	1.85	1000
Cs_2SnCl_6	9	2.50	2.50	2.16	1000
Cs_2TeCl_6	9	2.50	2.21	1.90	1000
Cs_2TiCl_6	9	2.50	2.34	2.12	1000

Br) is half metallic and semiconducting in the up and down spin states respectively [2]. Non-toxic, stable Rb_2(Os/Ir)(Cl/Br) $_6$ double perovskites with high polarization in both spins are attractive for spintronic devices and the 5d electrons of Os and Ir control their magnetic characteristics [3]. The results on electronic, optical and thermoelectric properties of Rb_2SeCl_6 and Rb_2TiCl_6 indicate their semiconducting character, light absorption from the visible to the ultraviolet region and figure of merit found as 0.74 and 0.76 [4]. The shifting of maximum absorption from visible to infrared region, the electrical, thermal conductivities and figure of merit of Cs_2TeX_6 (X = Cl, Br, I) demonstrate that the studied materials are excellent choice for probing solar cell and renewable energy applications [5]. The band gaps for Ga_2TiI_6 corresponding to the absorption in the entire visible region makes it an excellent material for solar cells [6]. An ab initio study was realized on the structural, mechanical, electronic, optical and thermoelectric characteristics of double halides perovskite Cs2CaSnX6 (X = Cl, Br, I) [7]. The double perovskite oxides M2YVO6 (M = Mg, Sr) are eloquent materials used for applications in optoelectronic devices [8]. DFT study on the structural, optoelectronic, thermodynamic, vibrational, and mechanical properties of Ruddlesden Popper (RP) perovskites Sr_2XO_4 (X = Zr, Hf) is made the framework of WIEN2K code [9]. It is reported that Cs_2SnCl_6 shows high stability characteristics at ambient environment [10–12]. A small A-site cation gives a wider band gap and any B-site element change (Ni, Pd, Pt, Se, Te) implies a band gap that depends on the size of the cation [13]. The experiment lattice constant of Cs_2SnCl_6 determined from X-ray diffraction is 10.3552 Å [14] and the Sn-Cl bond lengths are located in the range 2.402 Å to 2.423 Å [14]. Saadi Berri studied some properties of Cs_2BCl_6 (B = Se, Sn, Te, Ti) using the CASTEP code [15]. Ruosheng Zeng et al. studied the luminescence mechanism of Te^{4+}-doped Cs_2SnCl_6 lead-free perovskite [16]. Rehan Ullah et al. investigated the lattice constant and bulk modulus of Cs_2BCl_6 (B = Se, Sn, Te) using a semi-empirical model [17]. The electronic, optical, thermoelectric, and thermodynamic properties of Cs_2TiCl_6 double perovskite were studied using the WIEN2k code [18]. The thermoelectric properties of Cs_2TeCl_6 and Cs_2SnI_6 double perovskites were studied using WIEN2k code [19]. An empirical model allows M.G. Brik and I.V. Kityk to calculate the lattice constant, ionic radii and electronegativity experimental and theoretical for Cs_2BCl_6 (B = Sn, Se, Ti, Te) [20].

We present in this work a study on the morphology, thermodynamic and dynamical stability of the structure through interatomic distances, Helmholtz free energy and phonon frequencies. Our contribution extends to a detailed study of elastic, electronic, optical and thermoelectric characteristics of Cs_2MCl_6 (M = Se, Sn, Te and Ti) double perovskites. Our study indicates that these materials have high static dielectric constant and maximum real part in the ultraviolet energy range, which favor less the recombination rate of charge carriers and their use in optoelectronic devices. The adequate indirect band gap, high dielectric constants and absorption in ultraviolet energy, high static refractive index and high power conversion efficiency make these cubic double perovskites as ideal materials for solar cell applications. It is hoped that this work will motivate experimental researchers in this area of materials for applications in the photovoltaic and thermoelectric fields. The negativity of formation energy and Helmholtz free energy and no imaginary phonon modes throughout the Brillouin zone confirm the thermal, thermodynamic and dynamical stability of these double perovskites. Semiconductors Cs_2MCl_6 (M = Se, Sn, Te and Ti) double perovskites with flat conduction and valence bands, and an indirect band gap are p-type carriers. A high Seebeck coefficient, adequate ZT values

Table 2
Interatomic distances d_{Cl-Cs},d_{M-Cs},d_{M-Cl}, d_{Cl-Cl} of Cs_2MCl_6 (M = Se, Sn, Te and Ti) double perovskites.

	d_{Cl-Cs}(Å)	d_{M-Cs}(Å)	d_{M-Cl}(Å)	d_{Cl-Cl}(Å)
Cs_2SeCl_6	3,7876	4,6301	2,4414	3,4526
Cs_2SnCl_6Exp.	3,7818	4,6264	2,4886	3.5194
	3.665 [14]		2.423 [14]	3.896 [14]
Cs_2TeCl_6	3,8513	4,7135	2,5765	3,6437
Cs_2TiCl_6	3,7526	4,5836	2,3712	3,3534

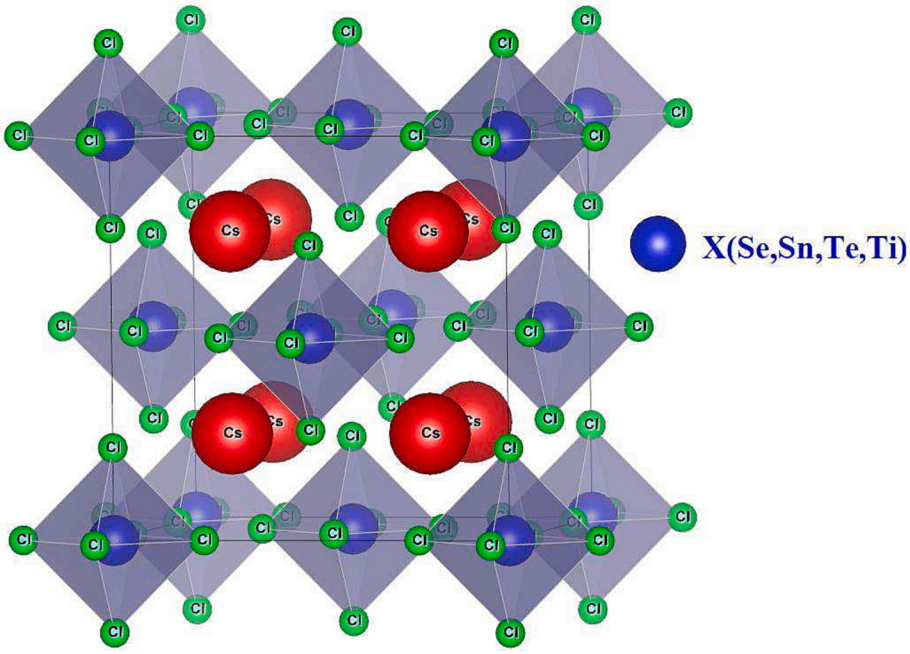

Fig. 1. The crystal structure of Cs2XCl6 (X = Sn, Se, Te and Ti) double perovskites.

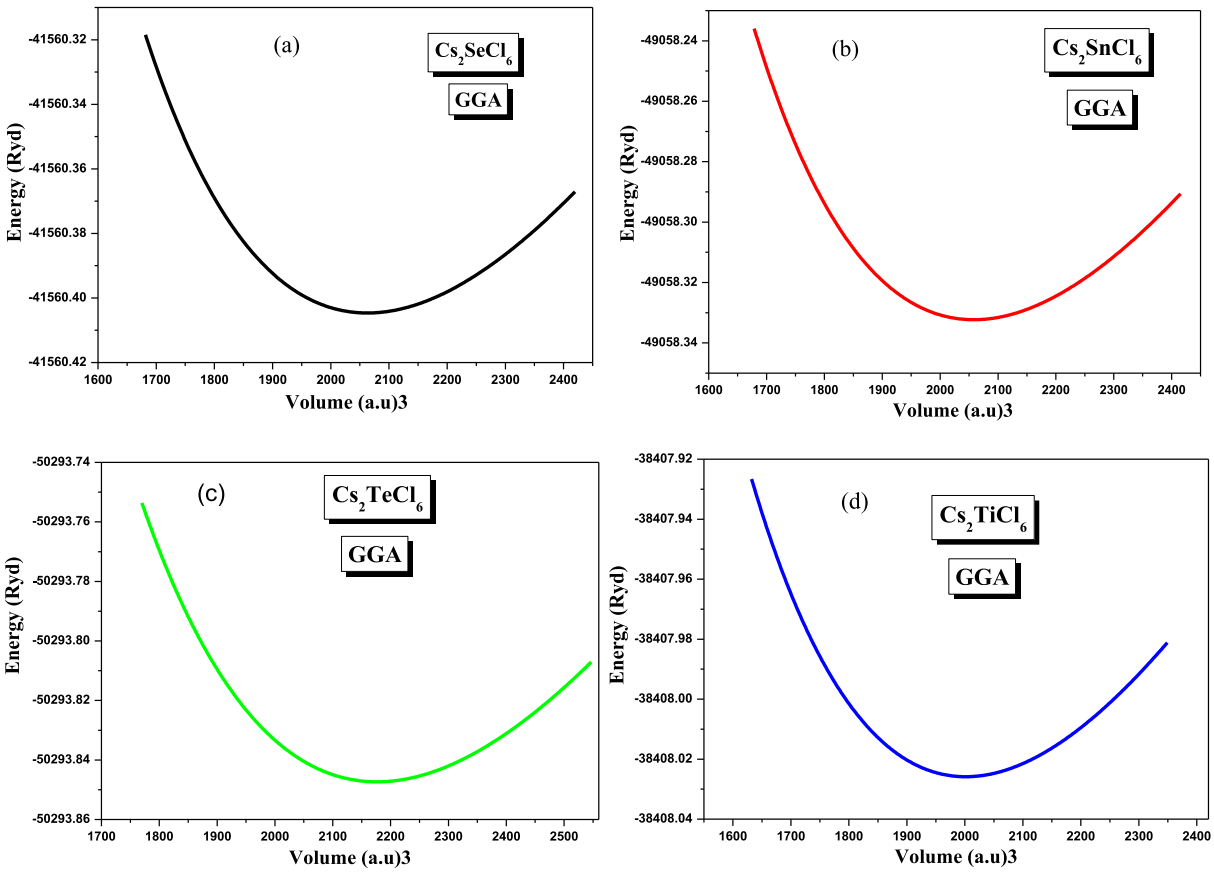

Fig. 2. Energy volume optimization curve of halide perovskites (a) Cs2SeCl6, (b) Cs2SnCl6, (c) Cs2TeCl6 (d) Cs2TiCl6 using GGA approximation.

Table 3
Calculated lattice constant (a_0), bulk modulus (B), pressure derivative of bulk modulus B' and minimum energy E_0.

	a_0 (Å)	B (GPa)	B'	E_0 (eV)
Cs_2SeCl_6	10.69	24.19	4.7686	-41560.404687
Exp.	10.26 [25]	33.24 [17]	5.00 [26]	-49032.239 [26]
Other	10.1853 [19]	29.589 [15]		
Cs_2SnCl_6	10.6841	26.966	4.9637	-49058.332356
Exp.	10.3562 [14]	32.21 [17]		
Other	10.646 [15]	33.175 [15]		
Cs_2TeCl_6	10.8853	24.8747	4.4762	-50293.847372
Exp.	10.445 [25]	31.27 [17]		
Other	10.5167 [19]	29.48 [19]		
Cs_2TiCl_6	10.5853	29.2259	4.6147	-38408.025908
Exp.	10.445 [14]	33.70 [17]		
Other	10.619 [15]	31.503 [15]		

and non-toxicity make these compounds attractive for thermoelectric applications at high temperature and spintronic technology.

Computational method

Based on density functional theory (DFT), all physical properties studied were carried out by utilizing Wien2k computational code [21]. The generalized gradient approximation (PBE-GGA) [22] from Perdew, Burke and Ernzerhof was used in the experimental lattice constant optimization process. The electronic and optical characterization were expected by the modified Becke-Johnson exchange potential [23], The electron–electron correlation effect is treated by the DFT + U [24]. To achieve perfect convergence of energy, the product of the smallest muffin-tin sphere radius (R_{MT}) and largest plane wave vector (K_{max}), $R_{MT}.K_{max}$ was taken as 9. The muffin-tin radii for Cs, Se, Sn, Te, Ti and Cl atoms were selected as mentioned in Table 1 for each double perovskites. Calculation of optical and thermoelectric properties requires k-meshes = 10000, while 5000 for elastic constants. The maximum radial expansion $I_{max} = 10$ is the value used for performing this self-consist calculations. The cut-off energy that separates valence and core states

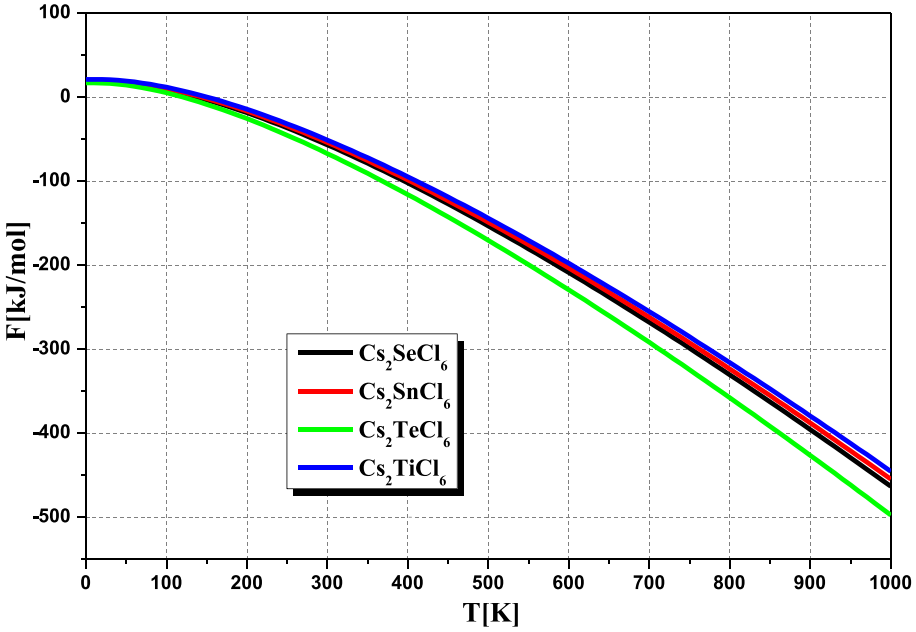

Fig. 3. Helmholtz free energy of Cs2XCl6 (X = Se, Sn, Te and Ti) as a function of temperature.

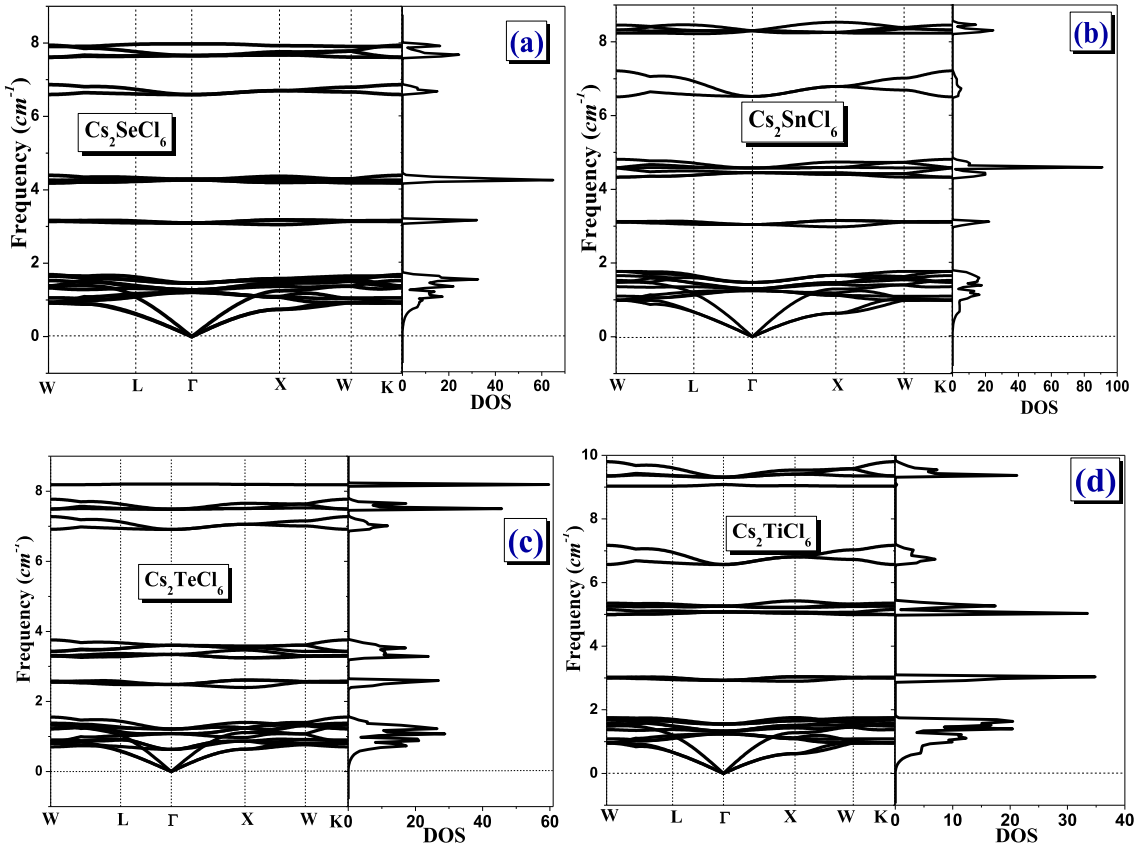

Fig. 4. Phonon band structures and DOS of Cs2XCl6 (X = Se, Sn, Te and Ti) using GGA-mBJ.

was − 8 Ry and 10^{-3} e was used as charge convergence. The conversion of waste heat into useful electric energy is described by figure of merit $ZT = \frac{S^2\sigma T}{k}$. S is the Seebeck coefficient,σ is electrical conductivity,k is thermal conductivity, and T is temperature. The total thermal conductivity is a combination of the lattice thermal conductivity (k_L) and electronic thermal conductivity (k_e).

$k_L = \frac{A\theta_D V^{1/3} m}{\gamma^2 n^{2/3} T}$,$A \approx 3.1 \times 10^{-6}$ is a physical constant,θ_D is the Debye temperature, γ is Grüneisen parameter,V is the volume per atom,n is the number of atoms in the primitive unit cell, and m is the average mass of the atoms in the crystal. Seebeck coefficient is given by:

$$S = \frac{8\pi^2 k_B^2 m^* T}{3eh^2}\left(\frac{\pi}{3n}\right)^{3/2}$$

k_B is the Boltzmann constant,m is the effective mass and n is the carrier concentration. The ratio of thermal to electrical conductivity is given by:$\frac{k}{\sigma} = \frac{\pi^2}{3}\left(\frac{k_B}{e}\right)^2 T$

Results and discussion

Crystal structure, morphology and stability

The crystal structure of Cs_2MCl_6 (M = Se, Sn, Te and Ti) double perovskites is shown in Fig. 1. Note that the M atoms (blue) reside in the octahedra formed by the Cl atoms (green), while the Cs atoms (red) occupy the interstitial sites. All of these double perovskites adopt the cubic structure with $Fm\bar{3}m$ space group symmetry. According to the crystal structure, the M − Cl, M−Cs, Cl-Cs and Cl-Cl bond lengths are reported in Table 2, with their available experimental data of Cs_2SnCl_6 [14]. The difference in the computed bond length is attributed to the electronegativity difference as well as the size of atoms. The M − Cl bond lengths are shorter and especially in the Cs_2TiCl_6 double perovskite, which reflects a strong interaction between M and Cl atoms and this is correlated with its better chemical stability. The stretching force in M−Cl bonds varies by changing the cation M. The constancy of the M−Cl, Cl-Cl, M−Cs and Cl-Cs bond lengths suggests the absence of major perturbation of the internal bonds. Fig. 2. sketch the diagram which illustrates the variation of energy as a function of volume and indicates their electronic stability. Table 3 lists calculated results for the optimized lattice constants, bulk modulus, pressure derivative of bulk modulus and and the corresponding minimum of cohesive total energy from equation of state Birch-Murnaghan. Our results agree well with their available experimental and theoretical data [14,15,17,19,25,26]. From the cohesive total energy, structural stability is more pronounced in the Cs_2TeCl_6 compound and less so in Cs_2TiCl_6.

Helmholtz free energy were calculated with harmonic approximation as a function of temperature as shown in Fig. 3. The negative value and the decrease of Helmholtz free energy when the temperature is enhanced for all double perovskites indicate the thermodynamic stability of these double perovskites. We display in Fig. 4 the phonon dispersion diagrams along some of the high symmetry lines of their corresponding Brillouin zones and total densities of state for Cs_2MCl_6 (M = Se, Sn, Te and Ti) double perovskites using GGA-mBJ functional. All compounds show no imaginary phonon modes throughout the Brillouin zone (all frequencies are positive) confirming the dynamical stability. The formation energy of Cs_2MCl_6 (M = Se, Sn, Te and Ti) is −2.77 eV, −3.11 eV, −2.84 eV and −3.83 eV, indicating their chemical stability.

Elastic constants and mechanical characteristics

The elastic parameters are obtained by solving the tensor matrix of the nonlinear equations using the Charpin method [27]. For cubic symmetry, the elements of the matrix are reduced to three C_{11}, C_{12} and C_{44} which are reported in Table 4, along with their mechanical characteristics estimated through these constants. The shear modulus, the bulk modulus as well as their Voigt and Reuss limits are reported in Table 4. The elastic constants and the bulk modulus satisfy the stability criteria $C_{11}+2C_{12}\rangle 0, C_{44}\rangle 0, C_{11}-C_{12}\rangle 0, C_{12}\langle B\langle C_{11}$ and therefore these double perovskites are mechanically stable. The lower elastic moduli mean that these double perovskites will be more easily deformed and will have less resistance to stretching or bending. The shear and bulk moduli, as well as their Voigt and Reuss limits of Cs_2SnCl_6 and Cs_2TeCl_6 are higher than those of Cs_2SeCl_6 and Cs_2TiCl_6. This implies that Cs_2SnCl_6 and Cs_2TeCl_6 are harder and stiffer compared with Cs_2SeCl_6 and Cs_2TiCl_6. It can be observed that elastic constants decrease in the sequence $Te \rightarrow Sn \rightarrow Se \rightarrow Ti$ due to larger ionic size of $Ti \rightarrow Se \rightarrow Sn \rightarrow Te$, and consequently these compounds become less rigid. Also, young's modulus confirms the larger resistance to uniaxial deformation in the

Table 4
Elastic constants, shear modulus, bulk modulus, anisotropy factor, Young's modulus, Poisson's ratio and B_H/G_H for Cs_2MCl_6 (M = Se, Sn, Te and Ti).

	Cs_2SeCl_6	Cs_2SnCl_6	Cs_2TeCl_6	Cs_2TiCl_6
C_{11} (GPa)	37.59	44.78	50.41	30.81
	63.21 [19]		59.92 [19]	42.53 [18]
C_{12} (GPa)	18.07	19.37	17.74	28.91
	15.46 [19]		14.14 [19]	16.78 [18]
C_{44} (GPa)	9.57	12.75	10.70	14.53
	9.67 [19]		6.92 [19]	10.82 [18]
G_v (GPa)	9.64	12.73	12.95	9.10
	15.35 [19]			
G_R (GPa)	9.64	12.73	12.42	2.15
	12.69 [19]			
G_H (GPa)	9.64	12.73	12.68	5.63
B_H (GPa)	24.58	27.84	28.63 [19]	29.55
	31.38 [19]		29.40 [19]	
A	0.98	1.00	0.65	15.32
	0.81 [19]		0.60 [19]	
E_V (GPa)	25.59	33.13	33.77	24.76
E_R (GPa)	25.59	33.14	32.55	6.32
E_H (GPa)	25.59	33.13	33.16	15.88
V_V	0.32	0.30	0.30	0.36
		0.30 [19]	0.32 [19]	
V_R	0.32	0.30	0.31	0. .46
V_H	0.32	0.30	0.30	0. .41
B_H/G_H	2.54	2.18	2.25	5.24
				2.19 [18]

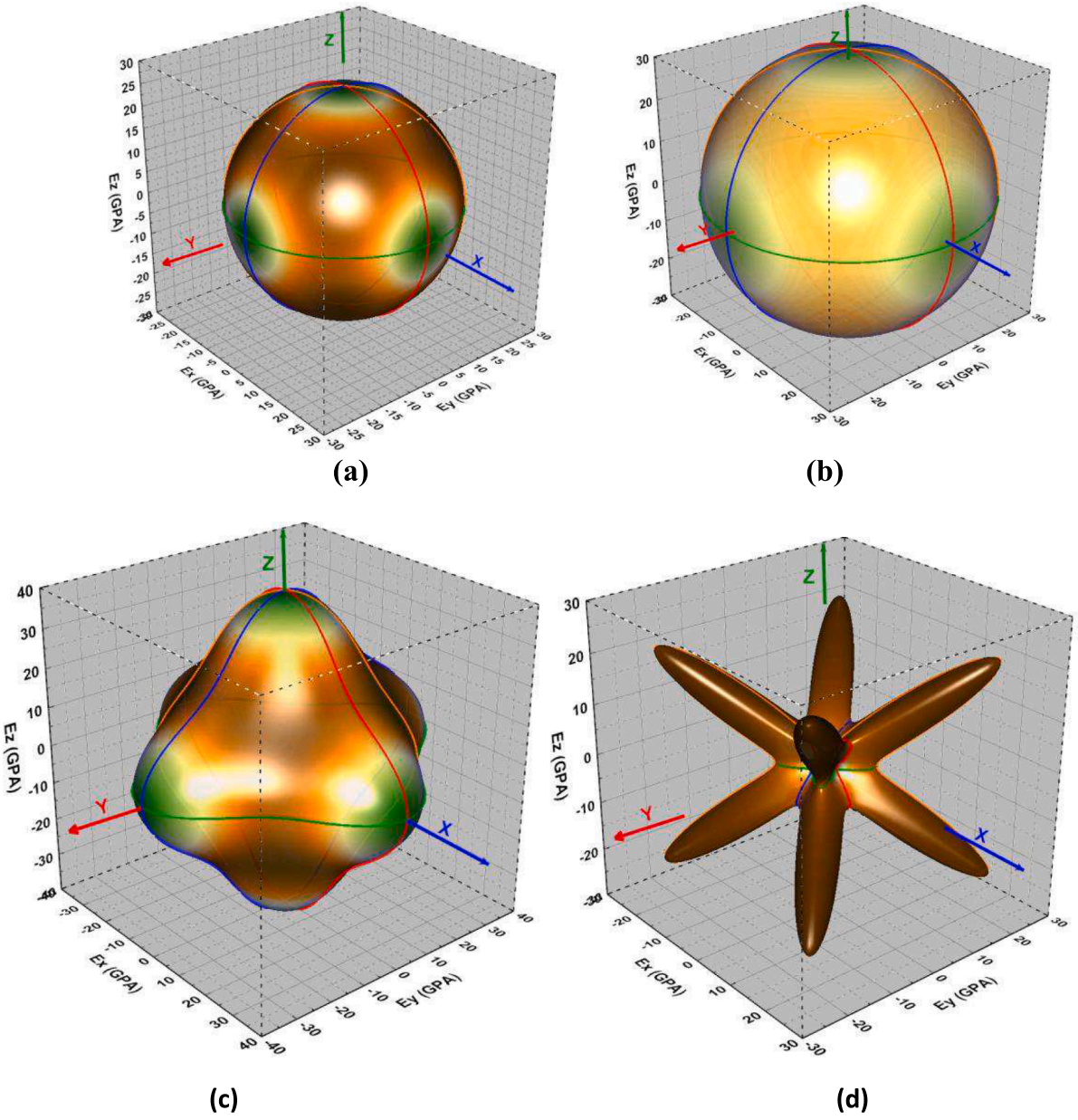

Fig. 5. The 3D surface construction of Young's modulus in Cs2SeCl6 (a), Cs2SnCl6 (b), Cs2TeCl6 (c) and Cs2TiCl6 (d) using GGA.

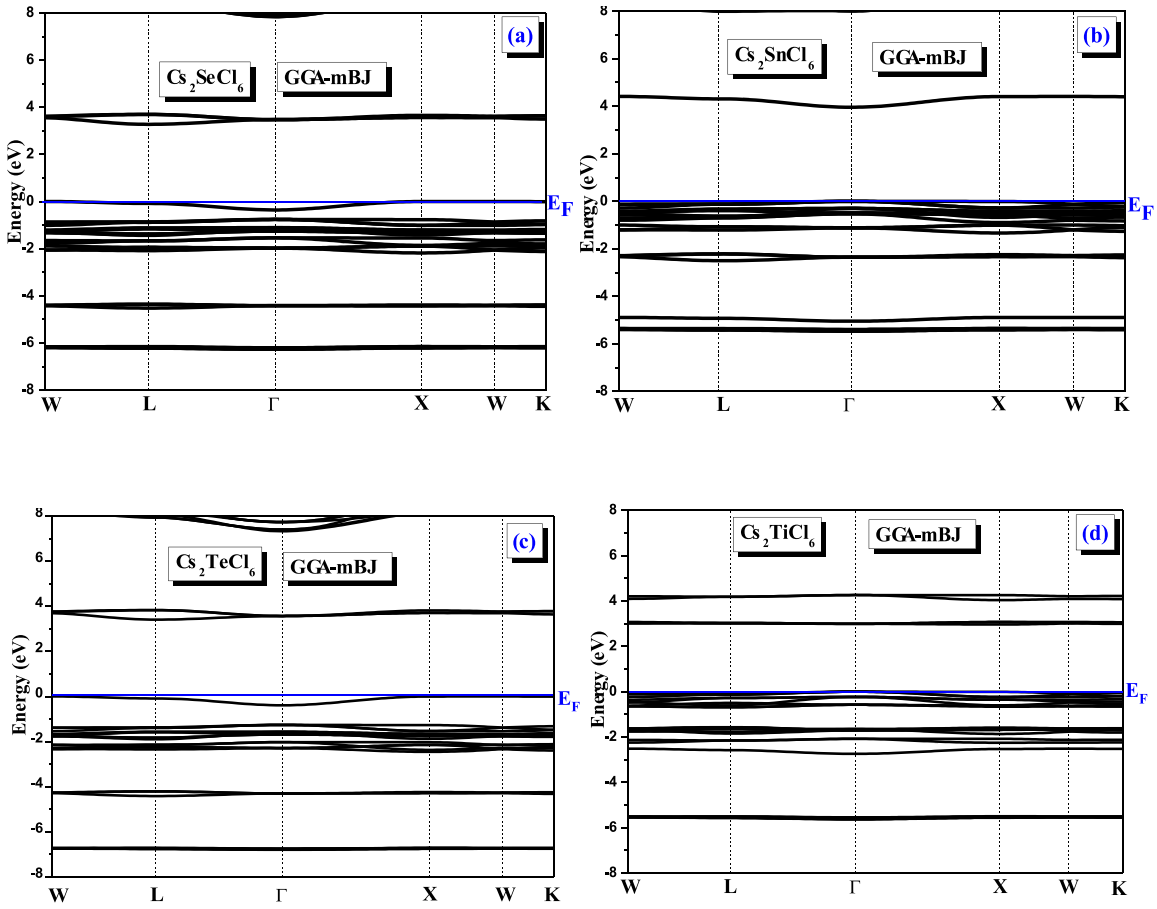

Fig. 6. The electronic band structures of Cs2MCl6 (M = Se, Sn, Te and Ti) using GGA-mBJ.

sequence *Te→Sn→Se→Ti*. We note that the bulk modulus is located between shear modulus and Young's modulus for each perovskite, signifying that all compounds allow uniaxial deformation more easily than volumetric deformation. The values of B/G ratio disclose the ductile nature of all the studied double perovskites. The values of Poisson's ratio $\nu > 0.25$ support forces as central type in all compounds. According to condition for anisotropy, Cs_2SnCl_6 is isotropic, while the others are anisotropic and the anisotropy is more pronounced in Cs_2TiCl_6. Fig. 5 shows the Young's modulus of Cs_2MCl_6 (M = Se, Sn, Te and Ti) double perovskites. It is presented by a contour along each graph in different directions using GGA-mBJ functional, where the unit is GPa. We note that Young's modulus is isotropic in Cs_2SeCl_6 and Cs_2SnCl_6 and anisotropic in the two others.

Electronic band structure and density of states

The electronic band structures of Cs_2MCl_6 (M = Se, Sn, Te and Ti) double perovskites were calculated using GGA, GGA-mBJ and EV-GGA, and are depicted in Fig. 6 along the high symmetry lines of the Brillouin-zone. It is noted that the profiles of the bands obtained are quite similar. Cs_2SnCl_6 shows an indirect W-Γ band gap, while the others have W-L indirect band gap character. The calculated band gaps are listed in Table 5, with their theoretical [18,19,26] and experimental [28,29] data. The GGA-mBJ gives band gap closer to the experimental value. Note that the top of the valence band of Cs_2SnCl_6 and Cs_2TiCl_6 is flat, suggesting a high effective hole mass and a large thermoelectric power. Better accuracy can be achieved with methods such as hybrid functionals, GW approximation and the modified Becke-Johnson functional. The modified Becke-Johnson functional is computationally less expensive and provides energy band gaps that are nearly equal to the experimental ones. For this reason, the optoelectronic and thermoelectric properties are studied employing the TB-mBJ functional as embedded in the WIEN2k code. The electronic configuration of Se, Sn, Te and Ti are $[Ar]3d^{10}4s^24p^4$, $[Kr]5s^24d^{10}5p^2$, [Ar] $4d^{10}5s^25p^4$ and [Ar] $3d^24s^2$. Then $4p^4$, $5p^2$, $5p^4$ and $3d^2$ states of the valence band for Cs_2SeCl_6, Cs_2SnCl_6, Cs_2TeCl_6 and Cs_2TiCl_6 are partially filled. The fundamental transitions in these double perovskites take place between 3p5 states of Cl and $4p^4$, $5p^2$, $5p^4$ and $3d^2$ states of Se, Sn, Te and Ti in Cs_2SeCl_6, Cs_2SnCl_6, Cs_2TeCl_6 and Cs_2TiCl_6. Therefore, the density of states predicts both the studied compounds as p-type semiconductors. An overview of the total and partial atomic density of states is shown in Fig. 7, where the Fermi level is set to 0 eV. The part located beyond the Fermi level, where the contribution is due to Se-p, Sn-p, Te-p and Ti-d shows hybridization with the Cl-p state. The empty first conduction band for mBJ-GGA corresponds to the band gap tabulated in Table 5. The possible transitions occur from Cl-p to (Se-p, Sn-p, Te-p and Ti-d). The observed wide band gap in these compounds is due to the hybridization of the *Cl −p* site and *Se −p, Sn −p, Te −p, Ti −d* states.

Table 5
The band gap of Cs_2MCl_6 (M = Se, Sn, Te and Ti) using GGA, GGA-mBJ, and EV-GGA.

	GGA	GGA-mBJ	EV-GGA	Other
Cs2SeCl6	2.76	3.28	2.76	3.9 [28] (exp.) 3.98 [26]
Cs_2SnCl_6	2.53	3.95	2.88	3.9 [29] (exp.)
s_2TeCl_6	2.78	3.41	2.926	3.10 [19]
Cs_2TiCl_6	2.24	2.96	2.39	2.87 [18]

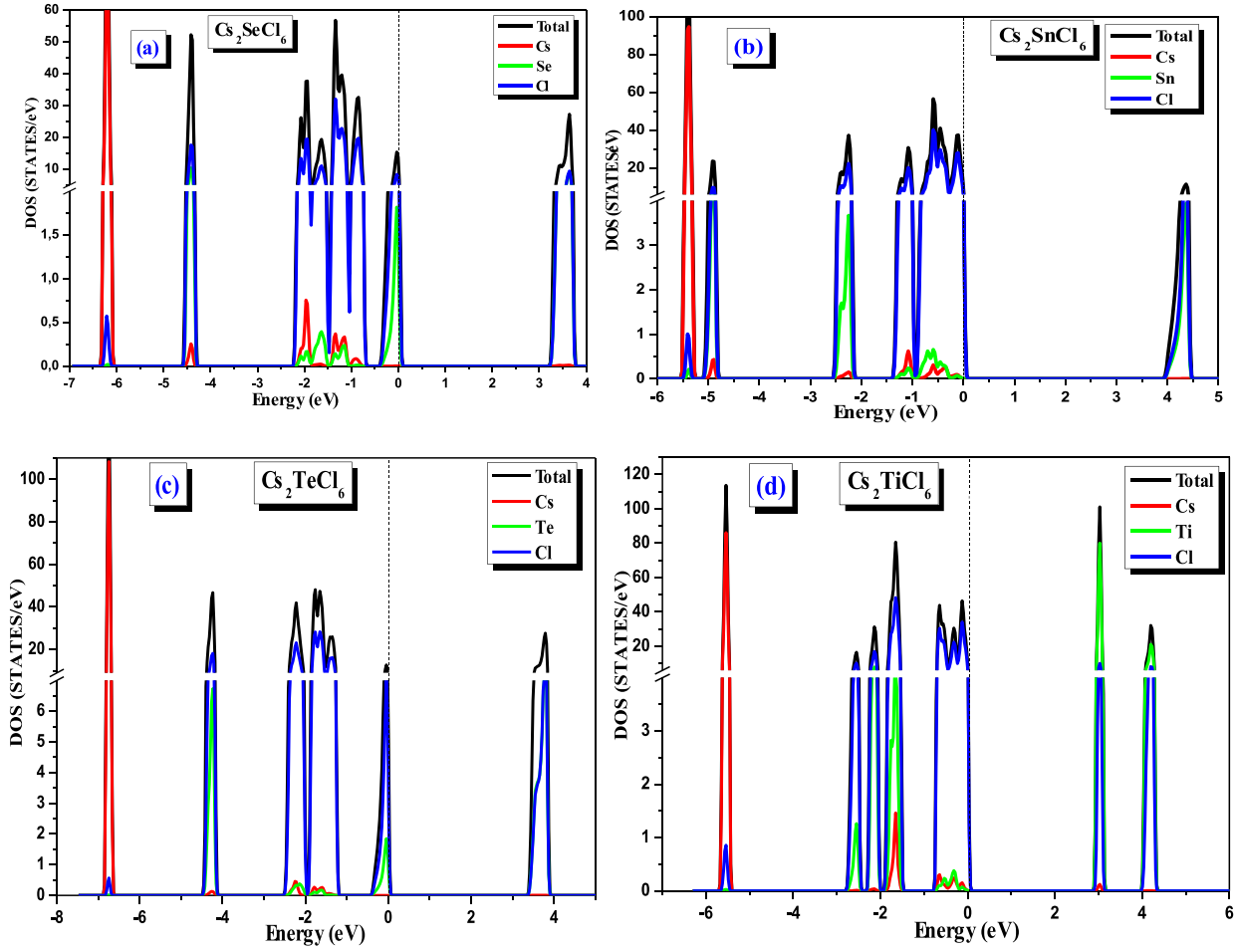

Fig. 7. The density of states of Cs2MCl6 (M = Se, Sn, Te and Ti) using GGA-mBJ.

Optical behavior

Fig. 8 visualizes the real (a) and imaginary (b) parts of the dielectric function, the refractive index (c), the extinction coefficient (d), the energy loss (e), the absorption coefficient (f), the reflectivity (g) and the optical conductivity (h) as a function of photon energy for Cs_2MCl_6 (M = Se, Sn, Te and Ti) double perovskites using GGA-mBJ. The dielectric function is treated by their real $\varepsilon_1(\omega)$ and imaginary $\varepsilon_2(\omega)$ parts, which respectively explains the electronic polarizability of a material and provides information about the absorption of a crystal. The spectra of real $\varepsilon_1(\omega)$ and imaginary $\varepsilon_2(\omega)$ parts show identical behavior, except for a slight shift towards high energies. The dielectric constant of a material is a measure of its ability to store electrical energy. It is an expression of the extent to which a material holds or concentrates electric flux. Dielectric constant is a characteristic of a material to reduce the electrostatic force acting between two charges. We note that the static dielectric constant is 3, 3.05, 4.4 and 4.8 for Cs_2TeCl_6, Cs_2SeCl_6, Cs_2SnCl_6 and Cs_2TiCl_6. Electrons located in semiconductors with covalent bonds induce a high dielectric constant and therefore high polarizability. The real part becomes negatve for an energy in the range 5 to 7 eV. This can be explained by the fact that the dielectric function has an excited field in opposite direction to the external field. This phenomenon occurs when the frequency of the external field is too low. We cannot compare these results due to the absence of experimental data in the literature. Charge carriers in semiconductors are determined by the static value of the dielectric function. A high static dielectric constant reduces charge carrier recombination with an intense peak in the real part of the dielectric function in the ultraviolet light make these double perovskites as candidate in optoelectronic devices. The imaginary part of the dielectric function reflects the amount of absorption inside the material and contributes to intra-band and inter-band transitions. The threshold energy called band gap is the first critical point which comes from the transition of electrons between the valence and conduction bands according to GGA-mBJ. The first peak of the imaginary dielectric constant corresponds to the band gap energy for all studied double perovskites. The refractive index describes the amount of light refracted in a material. The static refractive index is 1.75, 1.8, 2.12 and 2.20 for Cs_2TeCl_6, Cs_2SeCl_6, Cs_2SnCl_6 and Cs_2TiCl_6. It reaches a maximum value in the extreme ultraviolet region 2.16, 2.12, 3.7 and 2.6 and decreases faster when the speed of light is greater than the celerity of light (n = 1) and becomes negative at photon energy 4.5 eV to 7 eV. In this energy range, the response of materials changes from linear to non-linear. The extinction coefficient starts from the threshold energy. Cs_2MCl_6 (M = Se, Sn, Te and Ti) materials have strong extinction coefficient 2.25, 2.4, 2.12 and 1.75 near the ultraviolet region, then it decreases rapidly until it cancels out at photon energy located between 7 eV and 7.5 eV. The energy loss of fast electrons penetrating the materials under study depicts an intense peaks at photon energies between 4.5 and 5.5 eV for

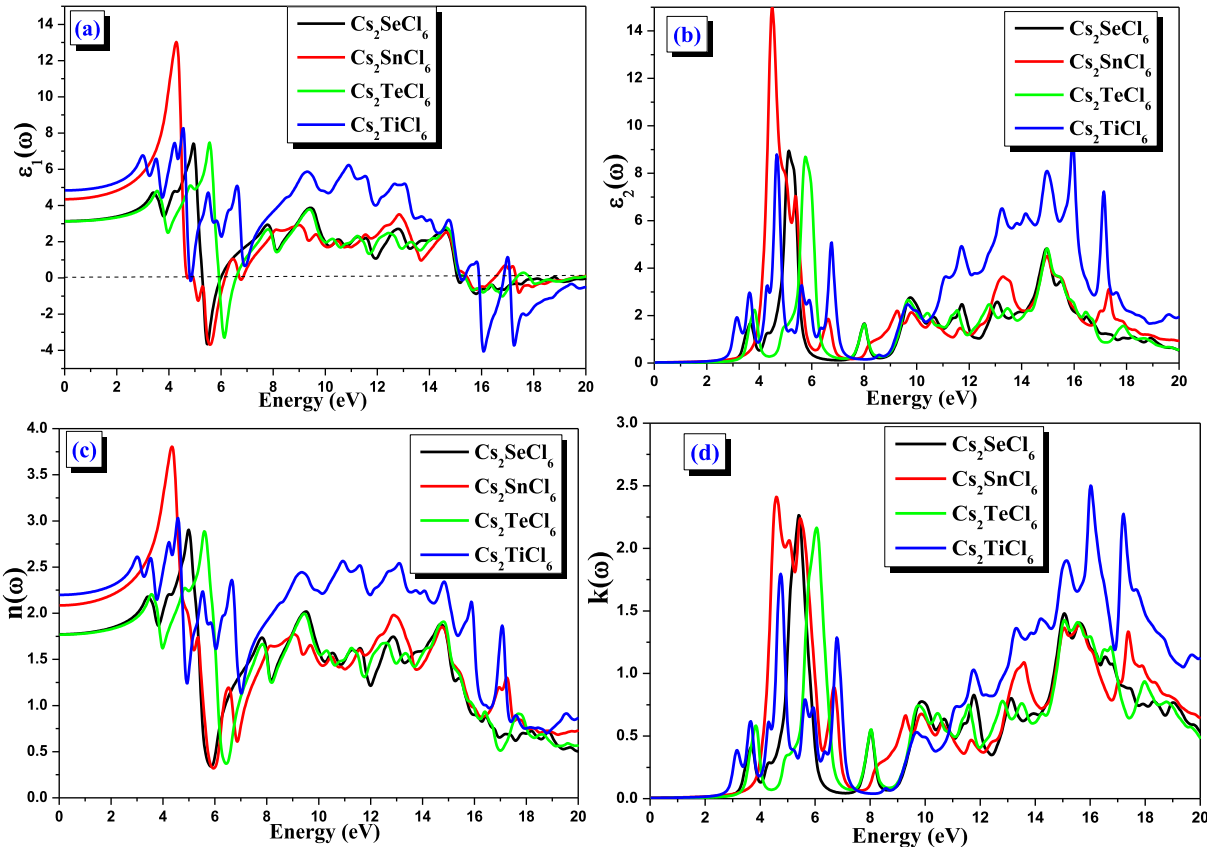

Fig. 8. The real (a) and imaginary (b) parts of the dielectric function, the refractive index (c), the extinction coefficient (d), the energy loss (e), the absorption coefficient (f), the reflectivity (g) and the optical conductivity (h) as a function of photon energy for Cs2MCl6 (M = Se, Sn, Te and Ti) double perovskites using GGA-mBJ.

Cs_2MCl_6 (M = Se, Sn, Te and Ti) double perovskites. These peaks linked to plasma resonance occur when the real dielectric constant is negative, with a rapid reduction in reflectance and the material becomes transparent. The first absorption region in the ultraviolet energy range was observed from 3 eV to 3.4 eV for Cs_2TiCl_6, 3.5 eV to 4.2 eV for Cs_2SnCl_6, 3.2 eV to 4 eV for Cs_2SeCl_6 and 3 eV to 4 eV for Cs_2TeCl_6. The theoretical report on absorption [18] 3.0 eV to 3.7 eV for Cs_2TiCl_6 was consistent with our result. The light absorption threshold 3.28 eV, 3.95 eV, 3.41 eV and 2.96 eV is identical to the optical band gap for Cs_2MCl_6 (M = Se, Sn, Te and Ti) using GGA-mBJ. The major peaks that exist in the absorption spectra correspond to the electronic transition from bonding states to the anti-bonding states. The static reflectivity values were noted as 7.5 %, 8 %, 12.5 % and 13 % for Cs_2MCl_6 (M = Te, Se, Sn and Ti) double perovskites. The reflectivity spectra have three parts, the first one in the range 0 to 3.0 eV, where the variation is almost linear, the second in the range 3.0 to 6 eV where the reflectivity passes through a set of maximum and minimum. The third part covers the energy range that corresponds to moderate reflectivity. The high dielectric constant and strong optical absorption are essential for better performance in solar cells. These characteristics were verified by the studied materials. Understanding transport characteristics requires elucidation of excitonic effects, electron-hole behavior and photogenerated effects. It is noted that the charges receive sufficient energy in order to be excited from the valence band towards the conduction band. The maximum of peaks is in the ultraviolet region of the photon spectrum.

Thermoelectric characteristics

Figs. 9, 10, 11 and 12 represent the thermoelectric response of Cs_2MCl_6 (M = Te, Se, Sn and Ti) double perovskites through the Seebeck coefficient, electrical conductivity, thermal conductivity and figure of merit as a function of chemical potential using the GGA-mBJ approach. These characteristics are calculated by the Boltzmann transport theory in the BoltzTraP code with a constant relaxtion time ($\tau = 10^{-14}$ s) [30]. A semiconductor shows better thermoelectric performance when the conduction and valence bands are flat [31], which is the case of our double perovskites under study. These materials are expected to have adequate thermoelectric characteristics. This is also explained by a more intense dispersion in the valence band near the Fermi level. The positive (negative) chemical potential $E-E_F$ corresponds to n-type (p-type) carriers. Seebeck coefficient is induced due to movement of both type of charge carriers. The n-type carriers give high Seebeck coefficient for all double perovskites studied. The Seebeck is high for energies above the Fermi level in all samples and decreases with increasing temperature. Seebeck coefficient is usually used to specify the majority carrier type and have an inverse relationship with electrical conductivity. The positive value of S confirms holes as majority carriers, and the negative values of S govern electrons as majority carriers. The electrical conductivity in semiconductors is due to electrons and holes. Electrical conductivity is a measure of the flow of electronic charge in a material. Negative (positive) values of $E-E_F$ represent *n*-type (p-type) charge carrier. For Cs_2SnCl_6, Cs_2TeCl_6 and Cs_2TiCl_6, the electrical conductivity

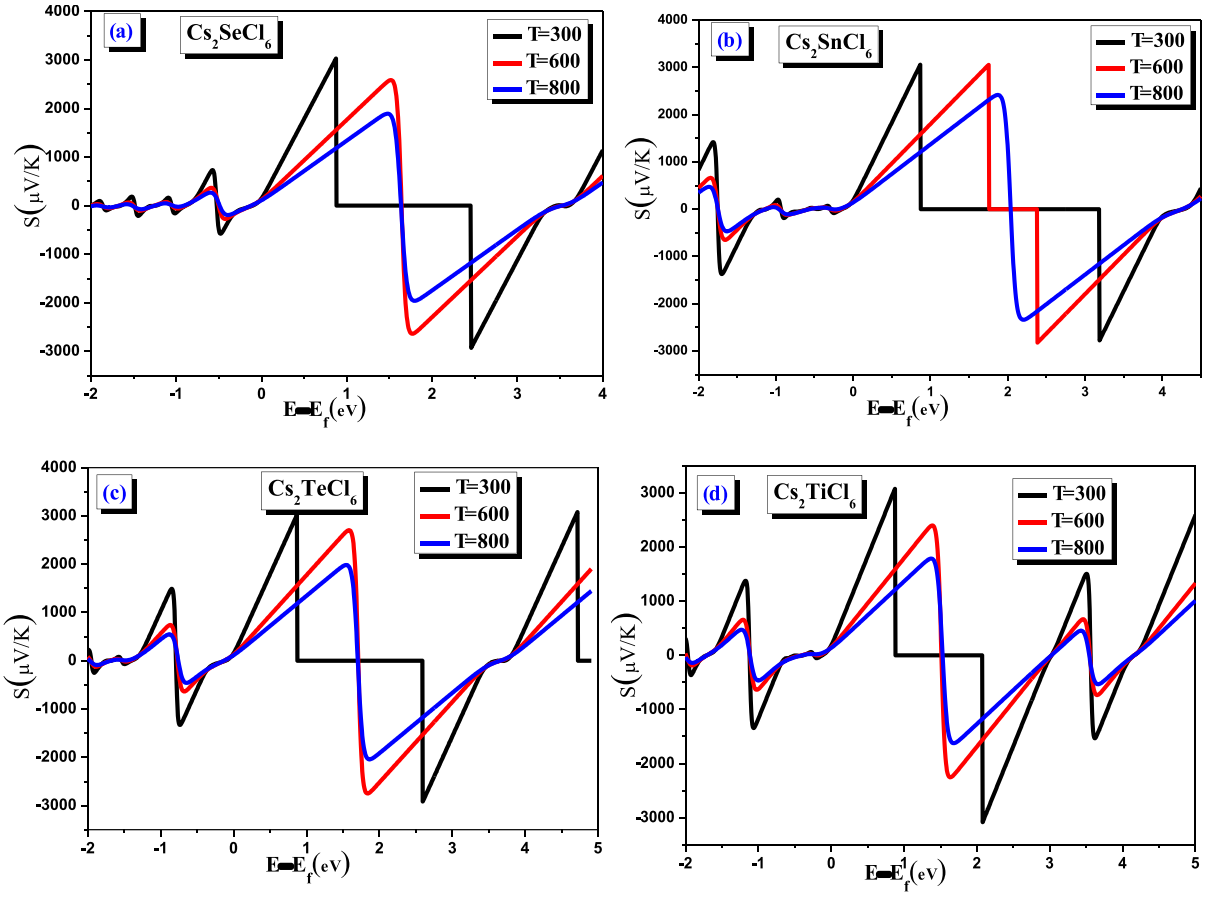

Fig. 9. Seebeck coefficient as a function of chemical potential at temperatures T = 300 K, 600 K and 800 K for (a) Cs2SeCl6, (b) Cs2SnCl6, (c) Cs2TeCl6 and (d) Cs2TiCl6 using GGA-mBJ.

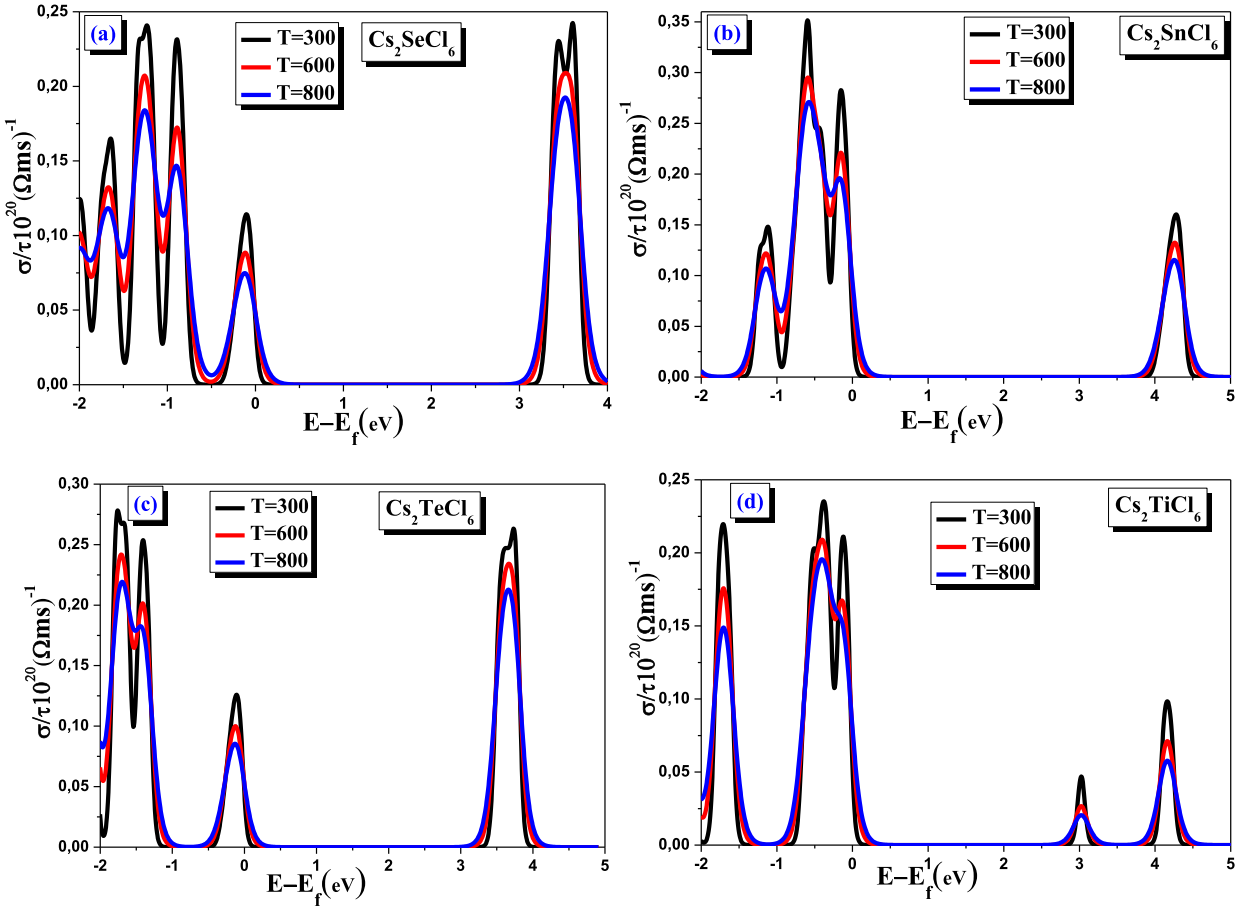

Fig. 10. Electrical conductivity as a function of chemical potential at temperatures T = 300 K, 600 K and 800 K for (a) Cs2SeCl6, (b) Cs2SnCl6, (c) Cs2TeCl6 and (d) Cs2TiCl6 using GGA-mBJ.

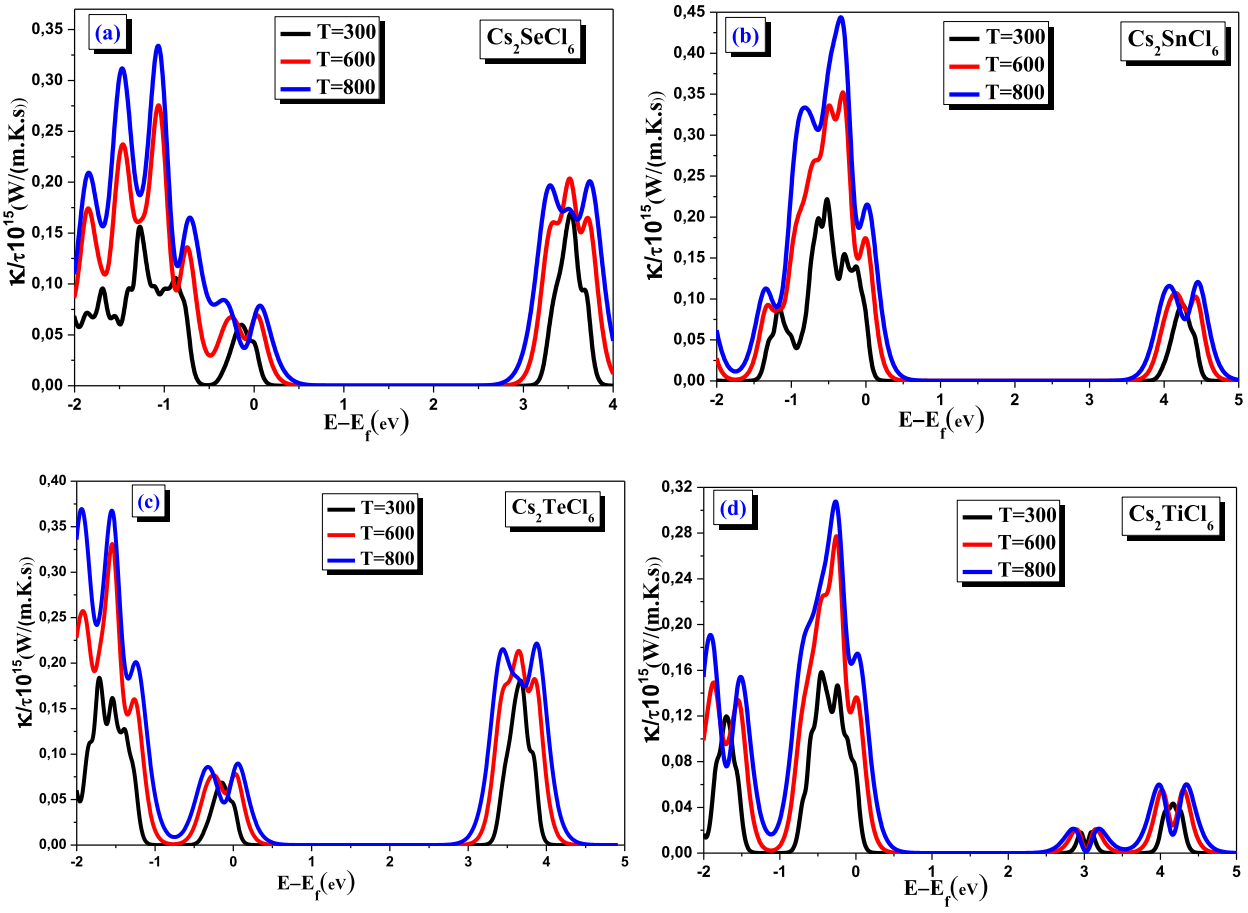

Fig. 11. Electronic thermal conductivity as a function of chemical potential at temperatures T = 300 K, 600 K and 800 K for (a) Cs2SeCl6, (b) Cs2SnCl6, (c) Cs2TeCl6 and (d) Cs2TiCl6 using GGA-mBJ.

due to electrons is greater than that of holes, while for Cs_2SeCl_6, the two type of conductivity are identical. Electrical conductivity decreases with increasing temperature, which increases the diffusion of charge carriers. The electrical conductivity for all double peovskites under study near the Fermi level at 300 K is approximately 2.5 x 10^4 $(\Omega ms)^{-1}$. No contribution to the electrical conductivity is observed in the studied double perovskites in the energy range 0 to 3 eV. Heat transfer in semiconductors is carried out by electrons and holes. There is no contribution to the electronic thermal conductivity for the studied double perovskites in the range 0.5 to 2.5 eV and next it starts increasing linearly. At the same temperature, the electronic thermal conductivity for p-type carriers is larger than that of n-type. The increase of electronic thermal conductivity when the temperature is enhanced is due to the increase corresponding in carriers mobility. The figure of merit describes the ability of a thermoelectric material in converting waste heat into useful electrical energy [32–36].

$$ZT = \frac{S^2 \sigma T}{k}$$

The figure of merit is expressed as a function of Seebeck coefficient, electrical conductivity, thermal conductivity and temperature. It is reported that a higher ZT value indicates the greater efficiency of a thermoelectric devices. The figure of merit is slightly sensitive to temperature and presents a maximum value close to unity in the important energy range. The peaks are more pronounced for p-type carriers than for n-type. A high Seebeck coefficient, adequate ZT values and non-toxicity make these compounds attractive for thermoelectric applications at high temperature and spintronic technology.

Conclusion

The calculated lattice constants of Cs_2MCl_6 (M = Se, Sn, Te and Ti) agree well with experiments values within 1.3 to 3 %. Cs_2SnCl_6 is isotropic, while the others are anisotropic and the anisotropy is more pronounced in Cs_2TiCl_6. The lower elastic moduli mean that these double perovskites will be more easily deformed and will have less resistance to stretching or bending. The Poisson's ratio values $\nu > 0.25$ support forces as central type in doubles perovskites under study. The systems Cs_2MCl_6 (M = Se, Sn, Te and Ti) show a W-Γ and W-L band gap, which increases from *Ti→Se→Te→Sn* using GGA-mBJ. The high dielectric constant and strong optical absorption in the ultraviolet light are essential for better performance in solar cells. The electronic thermal conductivity for p-type carriers is larger than that of n-type and its increase with temperature corresponds to the increase in carriers' mobility. The results on Cs_2MCl_6 (M = Se, Sn, Te and Ti) study indicate that these materials are a good absorption material due to their good stabilty, suitable band gap, and strong optical absorption. The density of states predicts all studied compounds as p-type semiconductors. A high Seebeck coefficient, adequate ZT values and non-toxicity make these compounds attractive for thermoelectric applications at high temperature and spintronic technology.

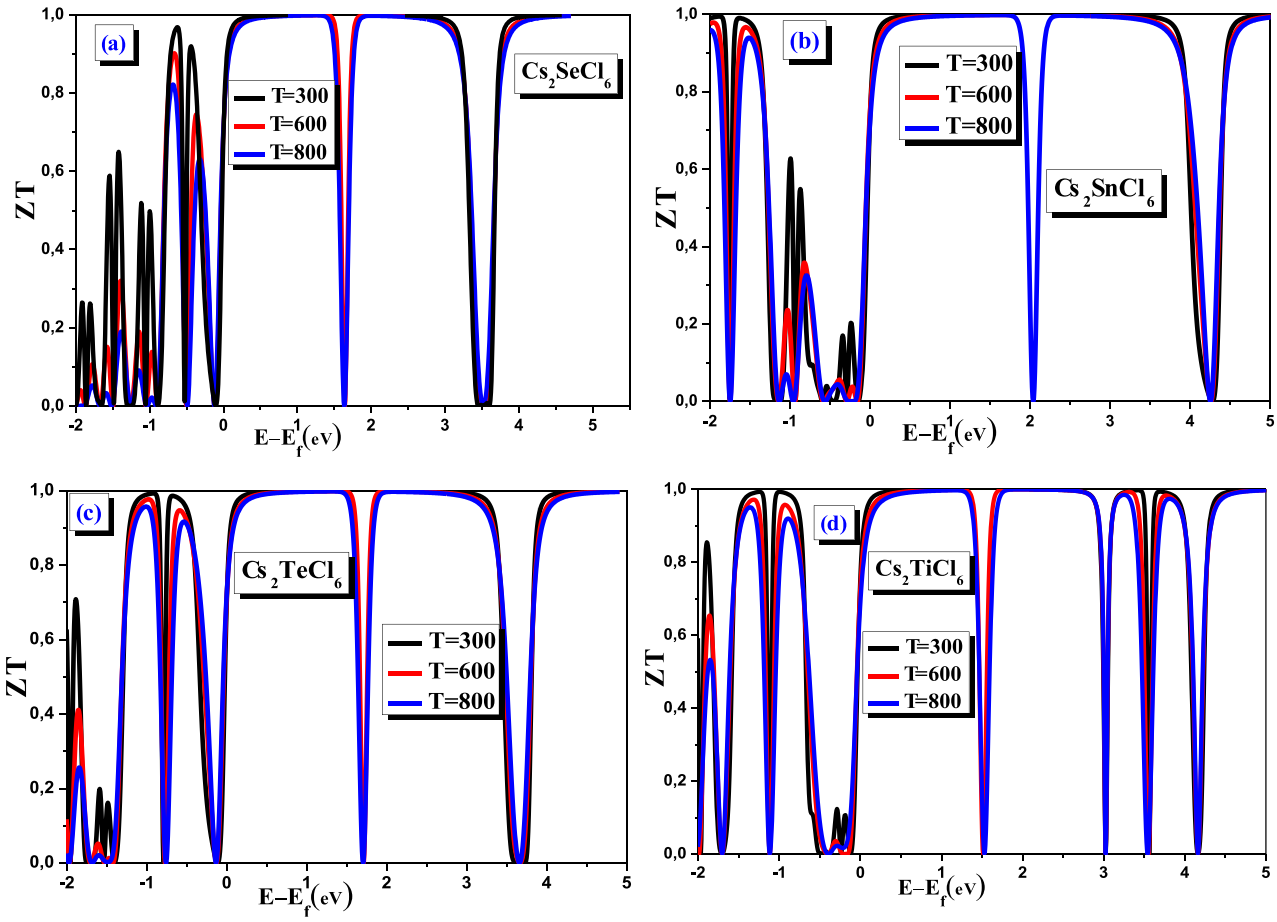

Fig. 12. Figure of merit as a function of chemical potential at temperatures t = 300 K, 600 K and 800 K for (a) Cs2SeCl6, (b) Cs2SnCl6, (c) Cs2TeCl6 and (d) Cs2TiCl6 using GGA-mBJ.

CRediT authorship contribution statement

K. Bouferrache: Investigation, Methodology, Project administration. **M.A. Ghebouli:** Project administration, Resources, Software, Supervision, Validation, Visualization. **B. Ghebouli:** Formal analysis, Funding acquisition, Investigation. **Mohamed A. Habila:** . **T. Chihi:** Data curation, Project administration. **M. Fatmi:** . **A. Djemli:** Formal analysis, Validation, Visualization. **Mika Sillanpaa:** .

Declaration of competing interest

The authors declare that they have no known competing financial interests or personal relationships that could have appeared to influence the work reported in this paper.

Data availability

The data that has been used is confidential.

Acknowledgements

This Work Was Funded by The Researchers Supporting Project Number (RSP2023R441), King Saud University, Riyadh, Saudi Arabia.

References

[1] Khuili M, Ouhammou A, Fazouan N, Atmani EH, Allaoui I, Al-Qaisi S, et al. Mod Phys Lett B 2023. https://doi.org/10.1142/S0217984923502238.
[2] Ali MA, Bahajjaj AAA, Al-Qaisi S, Sillanpää M, Khan A, Wang X. J Comput Chem 2023;44(23):1875–83. https://doi.org/10.1002/jcc.27166.
[3] Mustafa GM, Hassan M, Aloufi NM, Sadaf Saba S, AlQaisi QM, Hind Albalawi S, et al. Ceram Int 2022;48(16):23460–7. https://doi.org/10.1016/j.ceramint.2022.04.341.
[4] Al-Qaisi S, Mebed AM, Mushtaq M, Rai DP, Alrebdi TA, Sheikh RA, et al. J Comput Chem 2023;44(19):1690–703. https://doi.org/10.1002/jcc.27119.
[5] Albalawi H, Nazir G, Younas M, Al-Qaisi S, Ashiq MGB, Alzahrani J, et al. Phys Scr 2022;97:095801. https://doi.org/10.1088/1402-4896/ac831b.
[6] Al-Muhimeed TI, Alzahrani J, Rouf SA, Al-Qaisi S, Anbarasan R, Mahmood Q, et al. Phys Scr 2022;97:085815.
[7] Kiran S, Mumtaz U, Mustafa A, Imran M, Hussain F, Rasheed U, et al. Royal Society of Chemistry 2023;13:12925.
[8] Hussain MI, Khalil RMA. Mater Sci Semicond Process 2022;Vol. 152:107050. https://doi.org/10.1016/j.mssp.2022.107050.
[9] Arif Khalil RM, Hussain MI, Karim B, Albalawi H, Hussein KI, Hussain F, et al. Chemistry 2023;123:e27216.
[10] Lee B, Stoumpos CC, Zhou N, Hao F, Malliakas C, Yeh C-Y, et al. J Am Chem Soc 2014;136:15379–85.
[11] Saparov B, Sun J-P, Meng W, Xiao Z, Duan H-S, Gunawan O, et al. Chem Mater 2016;28:2315–22.
[12] Kaltzoglou A, Antoniadou M, Kontos AG, Stoumpos CC, Perganti D, Siranidi E, et al. J Phys Chem C 2016;120:11777–85.
[13] Cai Y, Xie W, Ding H, Chen Y, Thirumal K, Wong LH, et al. Chem Mater 2017;29:7740–9. https://doi.org/10.1021/acs.chemmater.7b02013.
[14] Thomas B, Gearhart CR, Welsh WA. J Magn Reson 1974;13:27–37.
[15] Berri S. J Phys Chem Solid 2022;170:110940. https://doi.org/10.1016/j.jpcs.2022.110940.

[16] Zeng R, Bai K, Wei Q, Chang T, Yan J, Ke B, et al. N Research 2021;14(5):1551–8. https://doi.org/10.1007/s12274-020-3214-x.
[17] Ullah R, Azmat Ali M, Katubi KMS, Alsaiari NS, Abualnaja KM, Verma AS, et al. Inorg Chem Commun 2022;139:109315.
[18] Mahmood Q, Hassan M, Yousaf N, AlObaid AA, Al-Muhimeed TI, Morsi M, et al. Mater Sci Semicond Process 2022;137:106180.
[19] Ali MA, Alshahrani T, Murtaza G. Mater Sci Semicond Process 2021;127:105728.
[20] Brik MG, Kityk IV. J Phys Chem Solid 2011;72:1256–60.
[21] P. Blaha, K. Schwarz, G. K. H. Madsen, D. Kvasnicka, WIEN2k: an augmented plane wave plus local orbitals program for calculating crystal properties, (2001).
[22] Burke K, Perdew JP, Ernzerhof M. J Chem Phys 1998;109(10):3760–71.
[23] Becke AD, Johnson ER. A Simple Effective Potential for Exchange. American Institute of Physics; 2006.
[24] Anisimov VI, Gunnarsson O. Phys Rev B 1991;43:7570.
[25] Engel G. Z Für Kristallogr - Cryst Mater 1935;90:341.
[26] Murtaza G, Hussain S, Faizan M, Khan S, Algrafy E, Ali MA, et al. Phys B Condens Matter 2020;595:412345.
[27] Mir SA, Gupta DC. RSC Adv 2020;10:26277.
[28] Dalpian GM, Liu Q, Stoumpos CC, Douvalis AP, Balasubramanian M, Kanatzidis MG, et al. Phys Rev Mater 2017;1:025401.
[29] Zeng R, Bai K, Wei Q, Chang T, Yan J, Ke B, et al. Nano Recherche 2021;14:1551–8.
[30] Madsen GKH, Singh DJ. Comput Phys Commun 2006;175:67–71.
[31] Haque E, Hossain MA. Results Phys 2018;10:458–65.
[32] Pei Y, Shi X, LaLonde A, Wang H, Chen L, Snyder GJ. Nature 2011;473:66.
[33] Chihi T, Fatmi M, Barka B, Ahmed SI, Sahnoune F. Results Phys 2019;14:102417.
[34] Ghebouli MA, Ghebouli B, Krache L, Alomairy S, Fatmi M, Chihi T, et al. Bull Mater Sci 2022;45(3):124.
[35] Bouferrache K, Ghebouli MA, Ghebouli B, Fatmi M, Alomairy S, Chihi T. Chin J Phys 2023;81:303.
[36] Bhat TM, Gupta DC. J Magn Magn Mater 2017;435:173.